Orientation behavior and deformation mechanism of polyethylene gels during cold drawing determined by in situ Raman spectroscopy

Orientation behavior and deformation mechanism of polyethylene gels during cold drawing determined by *in situ* Raman spectroscopy

Yusuke Hiejima, Takamasa Okuda, Koichi Kono and Koh-hei Nitta*

Department of Chemical and Materials Science, Kanazawa University, Kakuma Campus, Kanazawa 920-1192, Japan

In situ Raman spectroscopy has been used to investigate uniaxial stretching of polyethylene (PE) gels with various PE contents. Molecular orientation of the crystalline chains proceeds beyond the yield point and higher orientation is attained for PE gels with higher PE content, but orientation perpendicular to the stretching direction persists up to the highly stretched region. This biaxial orientation is essentially the same irrespective of the PE content, and it can be explained by the inhomogeneity embedded in the PE gel. The PE content dependence of the second-rank orientation parameter $<P_2>$ at high strain is similar to that of the dynamical mechanical properties, suggesting that the deformation mechanism is consistent during the entire stretching process from the elastic region to the highly stretched region.

*Corresponding author: nitta@se.kanazawa-u.ac.jp

Keywords: Polyethylene gel; Uniaxial stretching; *In situ* Raman spectroscopy

Introduction

Since formation of fibers with high modulus and strength from a polyethylene (PE) gel of ultra-high-molecular-weight polyethylene (UHMWPE) by drawing up to extremely high draw ratio was reported [1,2], there has been growing interest in the scientific and industrial aspects of PE gels. It has been found that gel drawing is suitable for producing highly oriented fibers and films. PE gels are formed by dissolving PE resin in solvents such as liquid paraffin and decalin followed by drawing at high extensional ratios. The uniaxially drawn fibers are highly oriented, and the modulus and strength are extremely high owing to the minimum network between lamellae crystallites, which are spontaneously formed under dilute conditions [3,4]. Because gel drawing produces porous structures with sizes of several dozens of nanometers, gel drawn films can be used as the separator films of small electronics and automotive batteries [5]. The gelation/crystallization mechanisms for generation of the cellular structure have been investigated. Quenched PE solutions show phase separation into PE-rich and PE-poor phases, followed by crystallization in the PE-rich phase [6,7].

Crystallization in bulk PE generates spherulitic structures, but the morphology in phase-separated systems strongly depends on the PE content: a single crystal mat is formed in dilute solution [8] and cellular structures composed of stacked lamellae are formed in semi-dilute or more concentrated solutions [9-11].

The superstructures undergo various deformations during cold drawing of bulk semi-crystalline polymers [12], such as fragmentation of lamellar crystals and subsequent fibrillation. The morphological and structural changes in PE gels during deformation have been investigated by scanning electron microscopy (SEM) and wide- and small-angle X-ray scattering (WAXD and SAXS) [13,14]. It has been reported that the sponge-like cellular structures in undrawn specimens are converted into fibrillar structures [2,9]. During gel drawing, the width of the crystallites appreciably decreases with increasing extensional ratio, resulting in a decrease in the fiber diameter [3].

Spectroscopic techniques are powerful tools for investigating the molecular structural changes in polymeric systems, because infrared and Raman spectroscopy are sensitive to microscopic structural changes in both the crystalline and amorphous phases [15-17]. Because the skeletal C–C stretching mode is strongly Raman active, microscopic deformation of the main chain of PE can be directly investigated by Raman spectroscopy. These spectroscopic techniques are also suitable for *in situ* measurements owing to the flexibility and versatility of the experimental setup. Because PE gels show substantial recovery after unloading the specimen owing to their elastic nature, *in situ* spectroscopic measurements of deformation at the molecular level give direct evidence of the intrinsic mechanism of deformation excluding the effect of stress relaxation after unloading the specimen.

The increase of the molecular weight between the entanglement points (M_e) in the amorphous phase of PE resin is responsible for the high drawability of PE gels. Because there is a power law relation between M_e and the volume fraction ϕ ($M_e \sim \phi^{-1.3}$) [18], a decrease of the PE content results in an increase of M_e. According to the elastic theory of rubbers, the maximum extensional ratio λ_{max} is proportional to $M_e^{0.5}$. The combination of these two relations predicts that $\lambda_{max} \sim \phi^{-0.65}$, which is consistent with the experimental observation that $\lambda_{max} \sim \phi^{-0.7}$ [19-22]. This suggests that an increase in the concentration of the PE resin results in an increase in entanglement [22], which influences the deformation mechanism during gel drawing.

In this study, we used Raman spectroscopy to monitor the molecular orientation of PE gels with various PE contents *in situ* during the entire stretching process. The orientation parameters were determined by polarized Raman spectroscopy and the orientation distribution of crystalline PE chains was also determined. We discuss the effect of the PE content on the mechanical and rheological properties, as well as the structure and morphology.

Experimental

High-density polyethylene (HDPE) with a molecular weight M_w = 3.0 × 10^5 and M_w/M_n = 6.0 (Toray Industries, Inc., Tokyo, Japan) was used as the resin. Liquid paraffin (LP) with M_w = 453 and kinetic viscosity of 50.7 mm^2/s was used as the solvent. Dibutylhydroxytoluene and ADK STAB AO-60 (ADEKA Cooperation, Tokyo, Japan) were added as antioxidants at concentrations of 1.0 and 0.7 wt% of the resin, respectively. The PE gel films were prepared by gelation/crystallization from solution as follows. The mixture of the PE resin, LP, and the antioxidants was kneaded at 100 rpm and 180°C for 5 min with a batch kneader. The kneaded PE solution was compression molded at 180°C and 20 MPa for 5 min using a laboratory hot press and then quenched at 25°C with a cold press. The thickness of the PE gel sheet was about 1 mm.

The dried PE gel films were prepared by removing LP as follows. Soxhlet extraction of the wet PE gel was performed with *n*-hexane as the extraction solvent for 24 h. The samples were then immersed in *p*-xylene to fill the cellular structures of the PE gels with the solvent. The PE gels were then immediately frozen in liquid nitrogen and dried under vacuum at 0 °C to sublimate *p*-xylene. The dried PE gels were obtained by drying under vacuum at 50 °C to remove the residual solvent.

The WAXD measurements of the dry and wet PE gels were performed with an X-ray diffractometer (RINT2500, Rigaku). Dynamic mechanical analysis (DMA) of the wet PE gels was performed with a dynamic mechanical analyzer (DVE-V4, UBM) at a frequency of 10 Hz in the temperature range from −150 to 140°C at a heating rate of 2 °C/min. Rectangular specimens with a width of 5 mm and a length of 30 mm were used. For the SEM observations, the dried PE gels were sputter-coated with Au–Pd alloy in vacuum, and the scanning electron microscope (S-4500, HITACHI) was operated at an accelerating voltage of 2.0 kV.

Table 1. Characteristics of the PE gels.

Sample code	PE conc. /wt%	LP conc. /wt%
PE/LP(29/71)	29	71
PE/LP(35/65)	35	65
PE/LP(42/58)	42	58
PE/LP(50/50)	50	50
PE/LP(57/43)	57	43
PE/LP(64/36)	64	36
PE/LP(70/30)	70	30

The uniaxial tensile tests of the wet PE gels were performed with a tensile machine (Model 4466, Instron) at 25°C and a strain rate of 0.5 min^{-1}. Dumbbell-shaped specimens with a gauge length of 6 mm and a width of 4 mm were cut from the PE gel sheets.

A rheo-Raman apparatus developed by ourselves was used in this study. The details of the experimental setup are described elsewhere [23,24]. A diode-pumped solid-state laser (RLK-640-200, LASOS) was used as the excitation light source. The wavelength and power of the laser were 639.7 nm and 200 mW, respectively. The laser was monochromated with a laser line filter and irradiated at the central portion of the specimen. A custom-made tensile machine with a double drawing mechanism was used for the tensile tests, and the laser spot was irradiated at the center of the specimen during the entire tensile test. Notch-shaped specimens with a gauge length of 2 mm and a width of 4 mm were cut from the wet PE gel sheets. The experiments were performed at 20°C with a strain rate of 0.5 min^{-1}. The backward-scattered light was collected and collimated with a pair of convex lenses into the optical fiber through a Raman long-pass filter. A charge-coupled device camera equipped with a monochromator (PIXIS100 and Spectra Pro 2300i, Princeton Instruments) was used as the detector. For the non-polarized measurements, a $\lambda/4$-wavelength plate was inserted in the excitation light path. The non-polarized Raman spectra were collected with an exposure time of 1 s and accumulated 10 times. For polarized Raman spectroscopy, a $\lambda/2$-wavelength plate and wire-grid polarizer were inserted in the optical path as the polarizer and analyzer, respectively. The polarized Raman spectra were accumulated 20 times with an exposure time of 1 s. The polarized states were *xx*, *yx*, and *yy* to the specimen, where the *x* axis is the stretching axis.

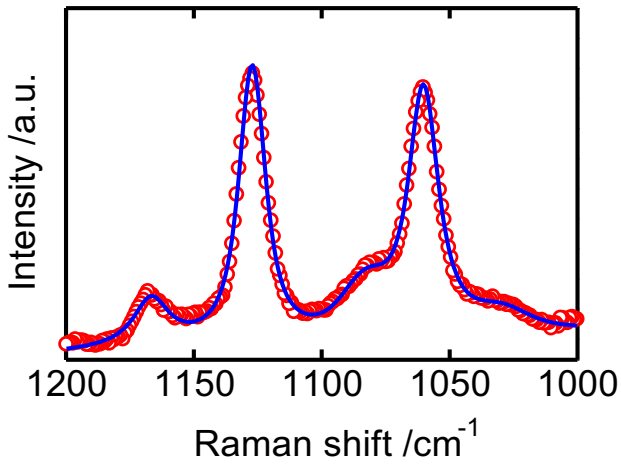

Fig. 1. Raman spectrum of PE/LP (42/58) (circles) and the fitted curve (solid line).

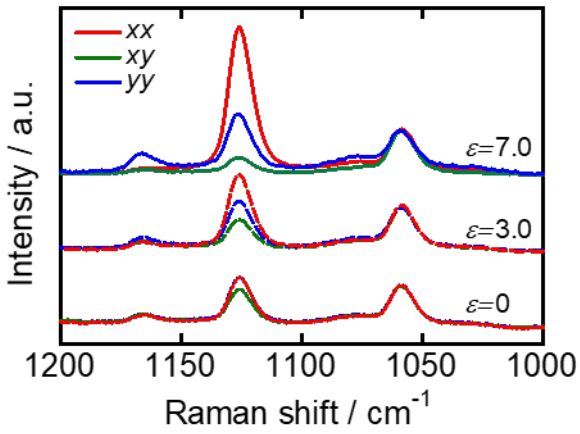

Fig. 2. *In situ* polarized Raman spectra of PE/LP (42/58) at various strains.

Table 2. Vibrational modes and phases for the Raman bands of PE [25-28].

Raman shift /cm^{-1}	Mode	Phase
1063	Anti-symmetric stretching (C-C)	Trans chain
1080	Stretching (C-C)	Amorphous
1130	Symmetric stretching (C-C)	Trans chain

The Raman spectrum of PE/LP (42/58) is shown in Fig. 1. The vibrational modes and phases of the PE resin are listed in Table 2. As shown in Fig. 1, the experimental Raman spectrum (circles) is successfully fitted by a sum of Voigt functions (solid curve). The polarized Raman spectra of PE/LP (42/58) at various strains under three polarization conditions are shown in Fig. 2. The 1063 cm^{-1} band assigned to the anti-symmetric stretching mode is not affected by the polarization conditions, but the 1130 cm^{-1} band under the *xx* geometry shows a much stronger peak than under the other conditions, indicating high orientation along the stretching direction (*x* axis).

The orientation parameters $\langle P_2 \rangle$ and $\langle P_4 \rangle$ as a function of the chain orientation angle θ with respect to the draw axis are given by [29]

$$\langle P_2 \rangle = \frac{3\langle \cos^2 \theta \rangle - 1}{2} \tag{1}$$

$$\langle P_4 \rangle = \frac{35\langle \cos^4 \theta \rangle - 30\langle \cos^2 \theta \rangle + 3}{8}. \tag{2}$$

These orientation parameters of the crystalline chains of the wet PE gel were determined using the intensities of the 1130 cm^{-1} band under the *xx*, *xy*, and *yy* geometries [23,30-32]. Although the amorphous band at 1080 cm^{-1} also shows appreciable polarization dependence, the Raman tensor for this band is not assigned to the A_g symmetry which is prerequisite for determining orientation parameters [29]. Note that we confirmed that the Raman spectrum of LP is appreciably weaker than

that of the PE gel, and no prominent peak is observed at around 1130 cm^{-1}. $\langle P_2 \rangle$ is a measure of the average orientation, and the combination of $\langle P_2 \rangle$ and $\langle P_4 \rangle$ enables us to describe the orientation distribution. The most probable value $\langle P_4 \rangle_{mp}$ for a given $\langle P_2 \rangle$ is approximately given by [29,33]

$$\langle P_4 \rangle_{\mathbf{mp}} = -0.083\langle P_2 \rangle + 1.366\langle P_2 \rangle^2 - 1.899\langle P_2 \rangle^3 + 1.616\langle P_2 \rangle^4 \tag{3}$$

for positive $\langle P_2 \rangle$, and

$$\langle P_4 \rangle_{\mathbf{mp}} = 0.052\langle P_2 \rangle + 1.574\langle P_2 \rangle^2 + 3.968\langle P_2 \rangle^3 + 8.057\langle P_2 \rangle^4 \tag{4}$$

for negative $\langle P_2 \rangle$. A $\langle P_4 \rangle$ value that is larger or smaller than the most probable value indicates that the orientation distribution is bimodal or unimodal, respectively [33,34].

The orientation distribution function (ODF) is expressed as a Legendre expansion as [33]

$$N(\theta) = \sum_{l=even} \left(\frac{2l+1}{2} \right) \langle P_l \rangle P_l(\cos\theta), \tag{5}$$

where $P_l(x)$ is the l-th Legendre polynomial. Although Raman spectroscopy only gives $\langle P_2 \rangle$ and $\langle P_4 \rangle$, the higher rank orientation parameters can be estimated by maximizing the information entropy of orientation. The most probable ODF is given by [24,29,33]

$$N(\theta) = \frac{\exp\left[\lambda_2 P_2(\cos\theta) + \lambda_4 P_4(\cos\theta) \right]}{\int_0^\pi \sin\theta \, d\theta \cdot \exp\left[\lambda_2 P_2(\cos\theta) + \lambda_4 P_4(\cos\theta) \right]}, \tag{6}$$

where λ_2 and λ_4 are the Lagrange multipliers determined to satisfy the following constraints for the experimental $\langle P_2 \rangle$ and $\langle P_4 \rangle$ values:

$$\langle P_l \rangle = \int_0^\pi \sin\theta \, d\theta \cdot P_l(\cos\theta) N(\theta) \quad (l = 2,4) \tag{7}$$

Results and discussion

SEM images of the dried PE gels before stretching are shown in Fig. 3. The dried PE gels have a cellular structure with cell sizes of ~1 μm, and the cell size slightly decreases with increasing PE content [11,35].

The WAXD profiles of the dried and wet PE gels along with that of bulk PE are shown in Fig. 4. The intensity of the amorphous halo for the PE gels is appreciably larger than that for bulk PE, but the crystalline peaks at $\theta = 21°$ from the (110) plane and 23° from the (200) plane are essentially the same, indicating that the crystalline structure of the PE resin is unaffected by gel formation. Then, it is likely that the wall of the cellular structure is mainly made of stacked lamellae, as demonstrated for PE gels formed in semi-dilute solutions [4,9].

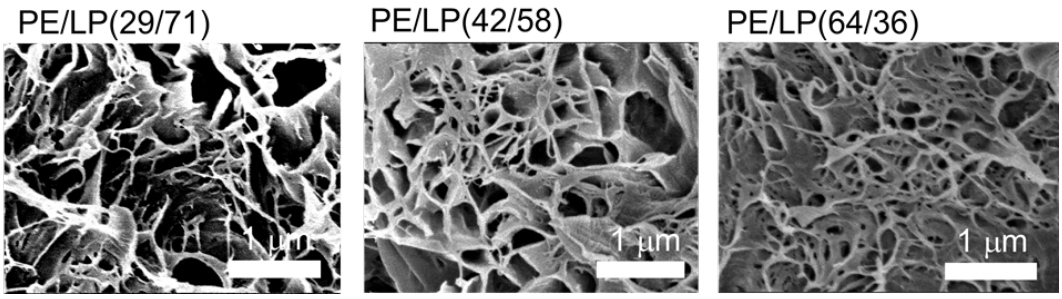

Fig. 3. SEM images of the dried PE gels before stretching.

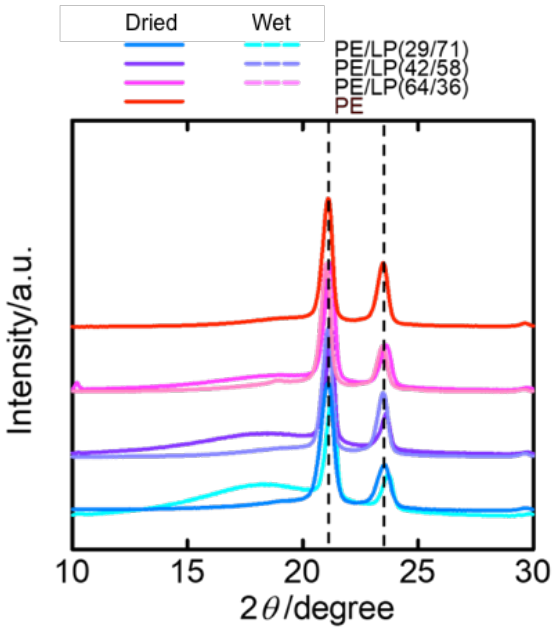

Fig. 4. WAXD profiles of bulk PE and the PE gels before (wet) and after (dried) extraction.

The dynamic mechanical spectra of the wet PE gels with various PE contents are shown in Fig. 5. The storage (E') and loss (E'') moduli gradually decrease with decreasing PE content, but the overall spectral shape is unchanged and tan δ is almost the same irrespective of the PE content, as shown in Fig. 5(b). The stress exerted on the PE gels is thus concentrated on the crystalline portion of PE. As shown in Fig. 5(c), the master curve obtained by the vertical shifts of E' and E'' can be expressed as

$$E'_{\mathrm{eff}} = b_\phi E', \quad E''_{\mathrm{eff}} = b_\phi E''. \tag{8}$$

The shift factor b_ϕ is plotted against the PE content in Fig. 5(d). The PE concentration dependence of the shift factor is given by a power law with an exponent of −1.5. This exponent is similar to that of the Young's modulus for open cell foam at sufficiently low relative density (−2.0) [36]. This suggests

that deformation of the PE gels at low strain can be interpreted as elastic deformation of the cellular structure in the PE gel.

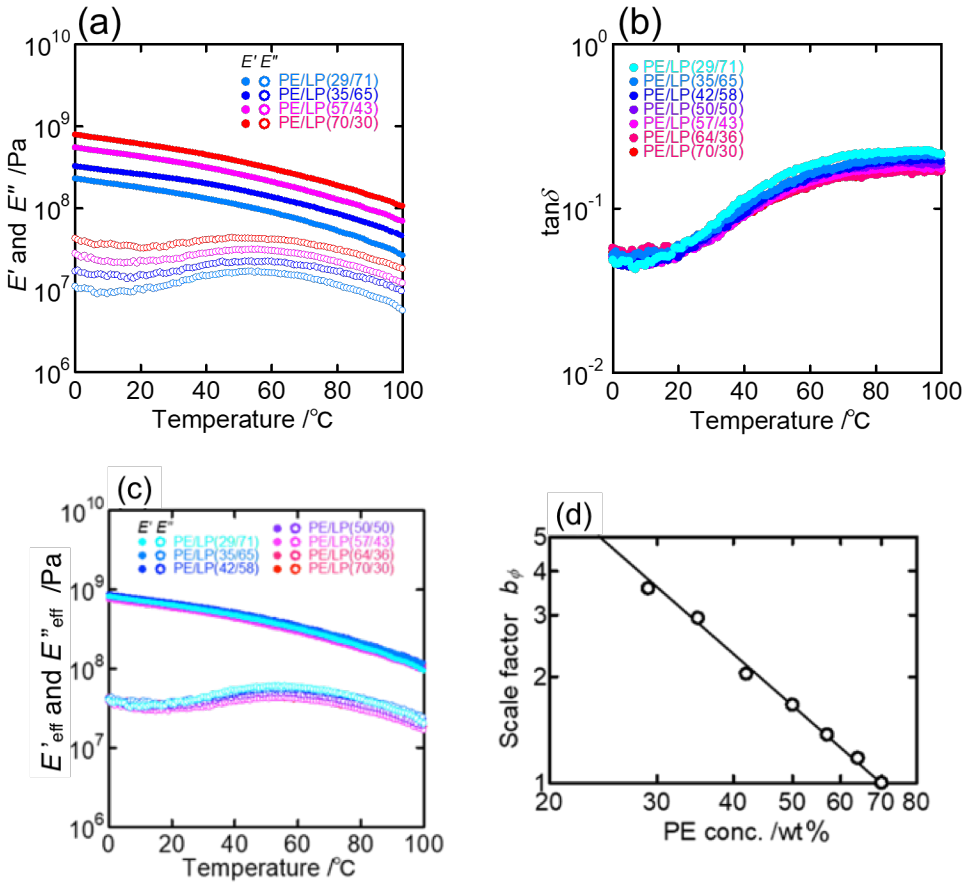

Fig. 5. Temperature dependence of (a) E' and E'' and (b) tan δ for PE gels with various PE contents. (c) Vertically shifted dynamic mechanical spectra. (d) Scale factor b_ϕ plotted against the PE content.

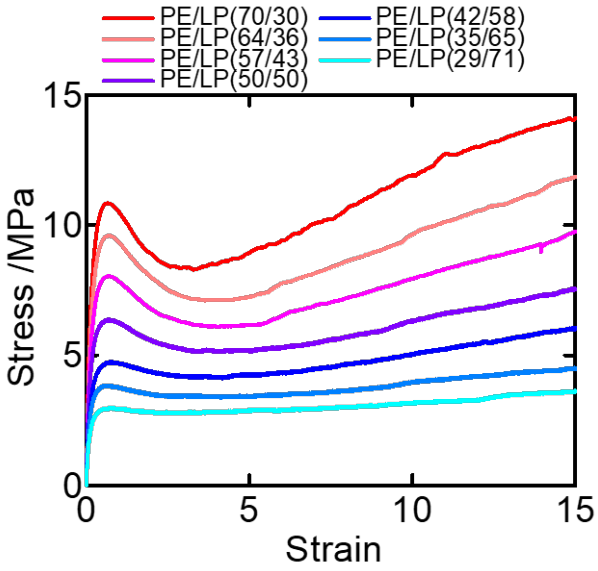

Fig. 6. Stress–strain curves of PE gels with various PE contents.

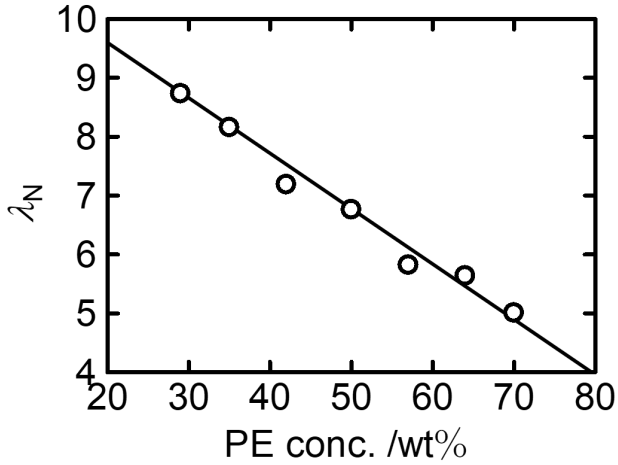

Fig. 7. PE concentration dependence of the natural draw ratio λ_N.

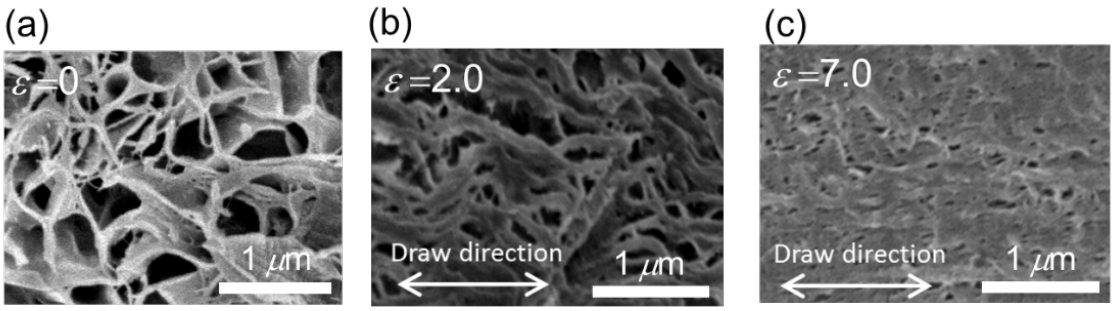

Fig. 8. SEM images of the dried gels of PE/LP (42/58) at (a) ε = 0, (b) ε = 2.0, and (c) ε = 7.0.

The stress–strain curves of the wet PE gels are shown in Fig. 6. Although the stress level clearly depends on the PE content, the overall behavior is similar to that of bulk PE, where the stress linearly increases until the yield point and then linearly increases again beyond the yielding region. Note that the notched specimen exhibits no necking plateau (see Fig. 6) because the neck expands into the entire portion of the gauge region immediately after the neck is initiated. The yield stress is approximately proportional to the PE content, suggesting that the exerted stress is solely loaded on the lamellae crystallites in the walls of the cellular structure. The yield stress decreases and the yield point becomes obscured with decreasing PE content, but the yield strain remains constant at ~1.3. The strain-hardening coefficient decreases with decreasing PE content, as previously reported [37]. Because the strain-hardening coefficient is proportional to the network density in the amorphous phase between oriented lamellae crystallites [38], the more gradual slope at lower PE content can be explained by lowering of the network density by dilution. The natural draw ratio λ_N determined by the Considère construction [12] is plotted against the PE content in Fig. 7. An increase of the PE content gives lower λ_N, suggesting enhancement of the crystalline orientation in the walls of the cellular structure.

SEM images of dried PE/LP (42/58) at various strains are shown in Fig. 8. Collapse of the cellular structure is observed beyond the yield point ($\varepsilon = 2.0$), followed by formation of a fibrillar structure at high strain of $\varepsilon = 7.0$. These observations indicate that the cellular structure begins to collapse at the yield point and the morphology transforms to a fibrillar structure in the highly stretched region. Similar morphological changes have been observed for UHMWPE gels [13]. The present interpretation is consistent with the SAXS/WAXD measurements [2,3], where fragmentation of the lamellar structure into a block-like structure is followed by formation of fibrillar structures aligned in the stretching direction.

The strain dependence of the orientation parameters and the stress–strain curves of the wet PE gels are shown in Fig. 9. In the elastic region, the orientation parameters $\langle P_2 \rangle$ and $\langle P_4 \rangle$ are essentially zero, indicating that the PE gels remain unoriented. Beyond the yield point, $\langle P_2 \rangle$ and $\langle P_4 \rangle$ increase with increasing strain, indicating the onset of molecular orientation. The onset strains are essentially the same, which is consistent with the fact that the yield strains are essentially constant. The $\langle P_4 \rangle$ values are clearly larger than the most probable values $\langle P_4 \rangle_{mp}$. The large $\langle P_4 \rangle$ values are characteristic of deformation of the PE gels, because $\langle P_4 \rangle$ is essentially the same as $\langle P_4 \rangle_{mp}$ for bulk PE, except for the yielding region where $\langle P_4 \rangle$ is appreciably lower than $\langle P_4 \rangle_{mp}$ [23,39]. Both $\langle P_2 \rangle$ and $\langle P_4 \rangle$ linearly increase with increasing strain beyond the yield point, but the slope is steeper for PE gels with higher PE content, indicating that molecular orientation proceeds at a higher rate, presumably because of the high concentration of entanglement points.

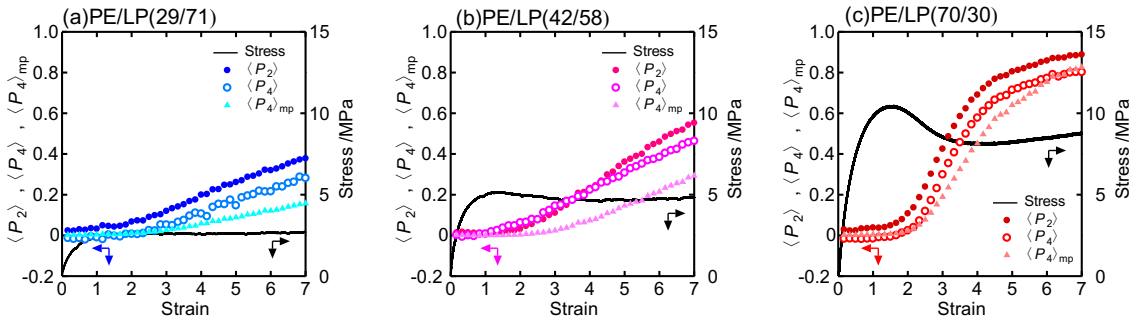

Fig. 9. Stress–strain curves and strain dependence of the orientation parameters for (a) PE/LP (29/71), (b) PE/LP (42/58), and (c) PE/LP (70/30).

The strain dependence of the orientation parameter $<P_2>$ for various PE contents is shown in Fig. 10. The onset of orientation is located at strain of about 1.3 irrespective of the PE content, as observed for the yield strain. Moreover, an increase in the PE content results in an increase in the rate of increase of $<P_2>$. We define the effective strain ε_{eff} as

$$\varepsilon_{\text{eff}} = \frac{\left(\varepsilon - \varepsilon_{\text{yield}}\right)}{a_\phi}, \tag{9}$$

where a_ϕ is a scale factor for orientation. Setting $a_\phi = 1$ for PE/LP (70/30) as a reference, the scale factors were determined to give the master curve in Fig. 10(b). The master curve suggests that addition of LP to the PE gel results in delay of orientation of the crystalline chains while maintaining the overall deformation mechanism. Considering that the natural draw ratio increases with decreasing PE content (see Fig. 7), it is plausible that a decrease in the effective strain of the PE matrix leads to an increase in the maximum draw ratio. In Fig. 10(c), the scale factor a_ϕ for the orientation parameter $<P_2>$ is plotted against the PE content and compared with scale factor b_ϕ from DMA analysis. Surprisingly, these two factors coincide, suggesting that the effect of the PE content on the deformation mechanism is consistent over the entire stretching process from the elastic region (DMA) to the highly deformed region ($<P_2>$). In order to clarify the precise physical meaning of the shift factors such as the plastic deformation, we need to characterize the localized strain under tension.

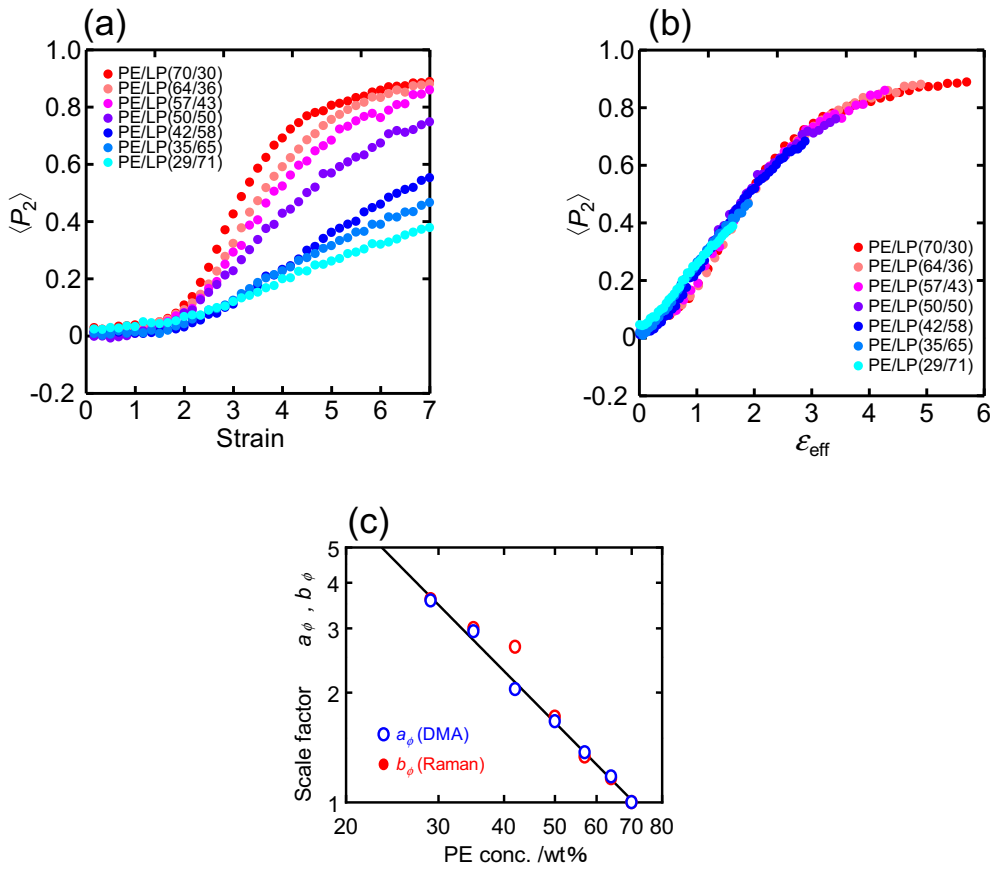

Fig. 10. Orientation parameter <P_2> plotted against (a) strain and (b) effective strain. (c) PE concentration dependence of scale factors a_ϕ and b_ϕ.

The ODFs for the wet PE gels are shown in Fig. 11. The ODF is constant irrespective of the polar angle up to strain of ~1, indicating random orientation. Beyond the yielding region, molecular chains oriented in the 30–60° direction from the stretching axis appreciably decrease, resulting in a biaxial orientation parallel and perpendicular to the stretching direction. The peak at $\theta = 0°$ becomes more prominent with increasing strain owing to evolution of the orientation with increasing strain, but the peak at $\theta = 90°$ persists even at high strain, indicating that biaxial orientation is maintained. Biaxial orientation is also observed for PE gels with high PE content, but the peak at $\theta = 0°$ becomes more prominent with increasing PE content. We have confirmed that the ODFs are consistent with the two-dimensional WAXD patterns of the stretched wet PE gels (see S-1 in Supporting Information),

though the biaxially-orientated pattern is weak presumably due to much lower orientation in the perpendicular direction ($\theta = 90°$) than along the stretching direction ($\theta = 0°$).

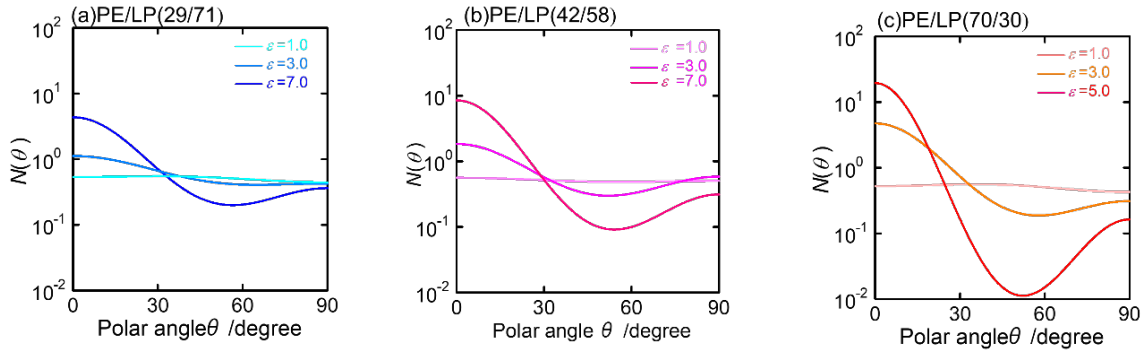

Fig. 11. ODFs at various strains for (a) PE/LP (29/71), (b) PE/LP (42/58), and (c) PE/LP (70/30).

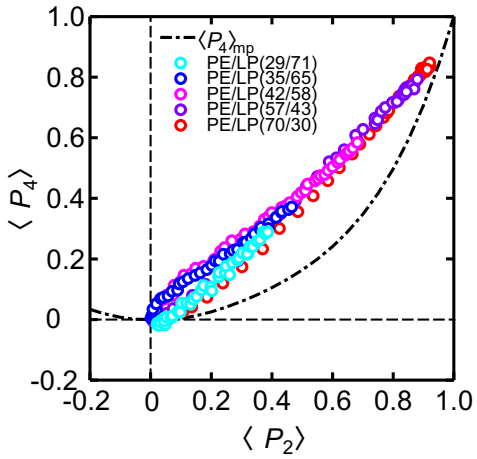

Fig. 12. $<P_2>$–$<P_4>$ diagram for PE gels with various PE contents during uniaxial stretching. The most probable values for $<P_4>$ calculated by Eqs. (3) and (4) are shown by the dot-dashed line.

The similarity of the orientation behavior of the wet PE gels is highlighted by the $<P_2>$–$<P_4>$ plot in Fig. 12. The relation between $<P_2>$ and $<P_4>$ is almost independent of the PE content, indicating that the overall mechanism of deformation is not affected by the PE content and the degree of orientation is suppressed with decreasing PE content. The $<P_4>$ values are markedly larger than the $<P_4>_{mp}$ values, indicating biaxial orientation. Biaxial orientation is not observed for bulk PE [23,24,39-41], suggesting that inhomogeneity in the wet PE gels is responsible for the orientation behavior; a portion of the lamellar crystals in the wall of the cellular structure remains somewhat undeformed.

The elastic deformation of the cellular structure is essentially unaffected by the PE contents,

because E' and E'' are scaled with vertical shifts with Eq. (9) and the yield strains remain unchanged. Although the crystalline orientation is suppressed by addition of LP, the deformation mode remains biaxial, presumably because of the intrinsic inhomogeneity of the stress transmission during stretching. It is plausible that the fluctuation caused by the inhomogeneity embedded in the PE gel leads to the cellular structure. Moreover, the PE content dependence of $<P_2>$ at high strains is scaled with an offset by the yield strain as Eq. (9). Considering the identical power law for the PE content dependence of these two scale factors (a_ϕ, $b_\phi \sim \phi^{-1.5}$), we suggest that the decrease in the effective strain with decreasing PE content in the post-yielding region simply results in depression of orientation without affecting the overall deformation mechanism.

Conclusions

In situ Raman spectroscopy has revealed the molecular orientation behavior of the crystalline chains in wet PE gels during uniaxial stretching. The orientation parameter $<P_2>$ begins to increase beyond the yield point, and it approaches an asymptotic value at high strain, indicating orientation toward the stretching direction. The $<P_2>$ value at high strain increases with increasing PE content, presumably because of enhancement of entanglement, but the approximately linear relation between $<P_2>$ and $<P_4>$ owing to biaxial orientation holds during the entire stretching process irrespective of the PE content. Biaxial orientation can be explained by inhomogeneous deformation in the cellular structure. The relevance of the cellular structure is supported by the power law with an exponent of ~1.5 for the PE content dependence of the shift factors for DMA analysis in the elastic region and $<P_2>$ in the highly stretched region, because it is close to that for elastic deformation of foams with low relative density of 2.0.

Acknowledgments

We would like to thank Toray Industries Inc. for experimental and financial support. We thank Edanz Group (www.edanzediting.com/ac) for editing a draft of this manuscript.

References

[1] P. Smith, P. Lemstra, B. Kalb, A. Pennings, Ultrahigh-strength polyethylene filaments by solution spinning and hot drawing, Polym Bull. 1 (1979) 733–736. doi:10.1007/BF00256272.

[2] P. Smith, P.J. Lemstra, J.P.L. Pijpers, A.M. Kiel, Ultra-drawing of high molecular weight polyethylene cast from solution, Colloid Polym Sci. 259 (1981) 1070–1080.

doi:10.1007/BF01524892.

[3] N.A.J.M. Van Aerle, A.W.M. Braam, A structural study on solid state drawing of solution-crystallized ultra-high molecular weight polyethylene, J Mater Sci. 23 (1988) 4429–4436. doi:10.1007/BF00551941.

[4] T. Ogita, R. Yamamoto, N. Suzuki, F. Ozaki, M. Matsuo, Molecular-weight dependence of morphology and mechanical properties of ultrahigh-molecular-weight polyethylene gel films, Polymer. 32 (1991) 822–834. doi:10.1016/0032-3861(91)90506-E.

[5] P. Arora, Z.J. Zhang, Battery Separators, Chem. Rev. 104 (2004) 4419–4462. doi:10.1021/cr020738u.

[6] Y. Luo, S. Kayakabe, Y. Xi, Y. Bin, C. Xu, M. Matsuo, Characteristics of several kinds of polyethylene gel estimated by small-angle light scattering under cross polarization, J. Polym. Sci. Part B: Polym. Phys. 49 (2010) 384–397. doi:10.1002/polb.22166.

[7] X. Shi, Y. Bin, D. Hou, Y. Men, M. Matsuo, Gelation/crystallization mechanisms of UHMWPE solutions and structures of ultradrawn gel films, Polym J. 46 (2014) 21–35. doi:10.1038/pj.2013.66.

[8] P.J. Barham, A. Keller, High-strength polyethylene fibres from solution and gel spinning, J Mater Sci. 20 (1985) 2281–2302. doi:10.1007/BF00556059.

[9] M. Kunz, R.E. De Micheli, M. Möller, An Electron Microscopic Study on the Formation of Polyethylene Fibrils, in: Integration of Fundamental Polymer Science and Technology—4, Springer Netherlands, Dordrecht, 1990: pp. 287–303. doi:10.1007/978-94-009-0767-6_34.

[10] D.R. Lloyd, S.S. Kim, K.E. Kinzer, Microporous membrane formation via thermally-induced phase separation. II. Liquid—liquid phase separation, J Membrane Sci. 64 (1991) 1–11. doi:10.1016/0376-7388(91)80073-F.

[11] S. Liu, C. Zhou, W. Yu, Phase separation and structure control in ultra-high molecular weight polyethylene microporous membrane, J Membrane Sci. 379 (2011) 268–278. doi:10.1016/j.memsci.2011.05.073.

[12] I.M. Ward, J. Sweeney, Mechanical Properties of Solid Polymers, 3rd ed., Wiley, 2013.

[13] M. Matsuo, C. Sawatari, T. Nakano, Ultradrawing of Isotactic Polypropylene Films Produced by Gelation/Crystallization from Solutions, Polym J. 18 (1986) 759–774. doi:10.1295/polymj.18.759.

[14] Y. Ikeda, T. Ohta, The influence of chain entanglement density on ultra-drawing behavior of ultra-high-molecular-weight polypropylene in the gel-casting method, Polymer. 49 (2008) 621–627. doi:10.1016/j.polymer.2007.11.043.

[15] M. Matsuo, T. Hashida, K. Tashiro, Y. Agari, Phase Separation of Ultrahigh Molecular Weight Isotactic Polypropylene Solutions in the Gelation Process Estimated in Relation to the Morphology and Mechanical Properties of the Resultant Dry Gel Films,

Macromolecules. 35 (2002) 3030–3040. doi:10.1021/ma011402.

[16] L. Berger, H.H. Kausch, C.J.G. Plummer, Structure and deformation mechanisms in UHMWPE-fibres, Polymer. 44 (2003) 5877–5884. doi:10.1016/S0032-3861(03)00536-6.

[17] Y. Hiejima, K. Takeda, K.-H. Nitta, Investigation of the Molecular Mechanisms of Melting and Crystallization of Isotactic Polypropylene by in Situ Raman Spectroscopy, Macromolecules. 50 (2017) 5867–5876. doi:10.1021/acs.macromol.7b00229.

[18] R.H. Colby, L.J. Fetters, W.G. Funk, W.W. Graessley, Effects of concentration and thermodynamic interaction on the viscoelastic properties of polymer solutions, Macromolecules. 24 (1991) 3873–3882. doi:10.1021/ma00013a021.

[19] R. Schaller, K. Feldman, P. Smith, T.A. Tervoort, High-Performance Polyethylene Fibers "Al Dente": Improved Gel-Spinning of Ultrahigh Molecular Weight Polyethylene Using Vegetable Oils, Macromolecules. 48 (2015) 8877–8884. doi:10.1021/acs.macromol.5b02211.

[20] P. Smith, P.J. Lemstra, H.C. Booij, Ultradrawing of high-molecular-weight polyethylene cast from solution. II. Influence of initial polymer concentration, J. Polym. Sci. Polym. Phys. Ed. 19 (1981) 877–888. doi:10.1002/pol.1981.180190514.

[21] T. Jian, W. De Shyu, Y.T. Lin, K.N. Chen, J.T. Yeh, Spinning and drawing properties of ultrahigh-molecular-weight polyethylene fibers prepared at varying concentrations and temperatures, Polym. Eng. Sci. 43 (2003) 1765–1777. doi:10.1002/pen.10149.

[22] L. Shen, J. Severn, C.W.M. Bastiaansen, Drawing behavior and mechanical properties of ultra-high molecular weight polyethylene blends with a linear polyethylene wax, Polymer. 153 (2018) 354–361. http://doi.org/10.1016/j.polymer.2018.01.083

[23] T. Kida, T. Oku, Y. Hiejima, K.-H. Nitta, Deformation mechanism of high-density polyethylene probed by in situ Raman spectroscopy, Polymer. 58 (2015) 88–95. doi:10.1016/j.polymer.2014.12.030.

[24] T. Kida, Y. Hiejima, K.H. Nitta, Molecular orientation behavior of isotactic polypropylene under uniaxial stretching by rheo-Raman spectroscopy, Express Polym Lett. 10 (2016) 701–709. doi:10.3144/expresspolymlett.2016.63.

[25] M.J. Gall, P.J. Hendra, O.J. Peacock, M.E.A. Cudby, H.A. Willis, The laser-Raman spectrum of polyethylene, Spectrochim Acta A: Mol Spectrosc. 28 (1972) 1485–1496. doi:10.1016/0584-8539(72)80118-1.

[26] M.J. Gall, P.J. Hendra, C.J. Peacock, M.E.A. Cudby, H.A. Willis, Laser-Raman spectrum of polyethylene: Part 1. Structure and analysis of the polymer, Polymer. 13 (1972) 104–108. doi:10.1016/S0032-3861(72)80003-X.

[27] R.T. Bailey, A.J. Hyde, J.J. Kim, J. McLeish, Raman studies on oriented, high modulus, polyethylene, Spectrochim Acta A: Mol Spectrosc. 33 (1977) 1053–1058.

doi:10.1016/0584-8539(77)80153-0.

[28] J.H. Schachtschneider, R.G. Snyder, Vibrational analysis of the n-paraffins—II, Spectrochim Acta. 19 (1963) 117–168. doi:10.1016/0371-1951(63)80096-X.

[29] D.I. Bower, Investigation of molecular orientation distributions by polarized raman scattering and polarized fluorescence, J. Polym. Sci. Polym. Phys. Ed. 10 (1972) 2135–2153. doi:10.1002/pol.1972.180101103.

[30] M. Pigeon, R.E. Prud'Homme, M. Pezolet, Characterization of Molecular-Orientation in Polyethylene by Raman-Spectroscopy, Macromolecules. 24 (1991) 5687–5694. doi:10.1021/ma00020a032.

[31] S. Frisk, R.M. Ikeda, D.B. Chase, J.F. Rabolt, Determination of the molecular orientation of poly(propylene terephthalate) fibers using polarized Raman spectroscopy: a comparison of methods, Appl Spectrosc. 58 (2004) 279–286. doi:10.1366/000370204322886618.

[32] M. Richard-Lacroix, C. Pellerin, Accurate New Method for Molecular Orientation Quantification Using Polarized Raman Spectroscopy, Macromolecules. 46 (2013) 5561–5569. doi: 10.1021/ma400955u.

[33] D.I. Bower, Orientation distribution functions for uniaxially oriented polymers, J Polym Sci Polym Phys Ed. 19 (1981) 93–107. doi: 10.1002/pol.1981.180190108.

[34] H. Pottel, W. Herreman, B.W. van der Meer, M. Ameloot, On the significance of the fourth-rank orientational order parameter of fluorophores in membranes, Chem Phys Lett. 102 (1986) 37–44. doi:10.1016/0301-0104(86)85115-1.

[35] L. Shen, M. Peng, F. Qiao, J.-L. Zhang, Preparation of Microporous Ultra High Molecular Weight Polyethylene (Uhmwpe) by Thermally Induced Phase Separation of a Uhmwpe/Liquid Paraffin Mixture, Chinese J. Polym. Sci. 26 (2008) 653–657. doi:10.1142/S0256767908003394.

[36] L.J. Gibson, M.F. Ashby, Cellular Solids: Structure and Properties 2nd edition, Cambridge (1999).

[37] O. Darras, R. Seguela, F. Rietsch, Dried gels from linear low-density polyethylene: Morphology, thermal behavior, and mechanical properties, J. Polym. Sci. Part B: Polym. Phys. 30 (1992) 349–359. doi:10.1002/polb.1992.090300405.

[38] R.N. Haward, Strain hardening of thermoplastics, Macromolecules. 26 (1993) 5860–5869. doi:10.1021/ma00074a006.

[39] Y. Hiejima, T. Kida, K.-H. Nitta, In Situ Monitoring of Orientation Parameters and Orientation Distribution Functions of Polyethylenes during Tensile Tests, Macromol. Symp. 377 (2018) 1700020. doi:10.1002/masy.201700020.

[40] T. Kida, Y. Hiejima, K.-H. Nitta, Rheo-optical Raman study of microscopic deformation in high-density polyethylene under hot drawing, Polymer Testing. 44 (2015) 30–36.

doi:10.1016/j.polymertesting.2015.03.018.

[41] T. Kida, Y. Hiejima, K.-H. Nitta, Rheo-Raman spectroscopic study of microscopic deformation behavior for ultra-low-density polyethylene, Polym. Int. 45 (2018) 1335–1340. doi:10.1002/pi.5533.